INTERNATIONAL JOURNAL OF HYDROGEN ENERGY 39 (2014) 16694–16705

Available online at www.sciencedirect.com

ScienceDirect

journal homepage: www.elsevier.com/locate/he

# Numerical evaluation of a PEM fuel cell with conventional flow fields adapted to tubular plates

J.M. Sierra [a,*], S.J. Figueroa-Ramírez [a], S.E. Díaz [a], J. Vargas [b], P.J. Sebastian [c]

[a] Facultad de Ingeniería, Universidad Autónoma del Carmen, Cd. del Carmen, Campeche C.P. 24115, Mexico
[b] Instituto de Investigaciones en Materiales, Unidad Morelia, Universidad Nacional Autónoma de México, Antigua Carretera a Pátzcuaro No. 8701, Col. Ex Hacienda de San José de la Huerta, C.P. 58190 Morelia, Michoacán, Mexico
[c] Instituto de Energías Renovables, Universidad Nacional Autónoma de México, Temixco, Morelos C.P. 62580, Mexico

ARTICLE INFO

*Article history:*
Available online 21 May 2014

*Keywords:*
PEM fuel cell
Tubular design
Flow field
CFD

ABSTRACT

In this research a 3D numerical study on a PEM fuel cell model with tubular plates is presented. The study is focused on the performance evaluation of three flow fields with cylindrical geometry (serpentine, interdigitated and straight channels) in a fuel cell. These designs are proposed not only with the aim to reduce the pressure losses that conventional designs exhibit with rectangular flow fields but also to improve the mass transport processes that take place in the fuel cell cathode. A commercial computational fluid dynamics (CFD) code was used to solve the numerical model. From the numerical solution of the fluid mechanics equations and the electrochemical model of Butler-Volmer different analysis of pressure losses, species concentration, current density, temperature and ionic conductivity were carried out. The results were obtained at the flow channels and the catalyst layers as well as in the gas diffusion layers and the membrane interfaces. Numerical results showed that cylindrical channel configurations reduced the pressure losses in the cell due to the gradual reduction of the angle at the flow path and the twist of the channel, thus facilitating the expulsion of liquid water from the gas diffusion layers and in turn promoting a high oxygen concentration at the triple phase boundary of the catalyst layers. Moreover, numerical results were compared to polarization curves and the literature data reported for similar designs. These results demonstrated that conventional flow field designs applied to conventional tubular plates have some advantages over the rectangular designs, such as uniform pressure and current density distributions among others, therefore they could be considered for fuel cell designs in portable applications.


## Introduction

One of the most promising technologies at the new hydrogen economy are the fuel cells. These are characterized by their high conversion efficiency, modularity and zero pollution. Their advantages have made them a leading technology that can replace the internal combustion engines in transportation and batteries in portable applications [1]. Currently there are different types of fuel cells, which are distinguished by the

* *Corresponding author*. Tel.: +52 9383896111.
E-mail addresses: jsierra@pampano.unacar.mx, juanmsg@live.com.mx (J.M. Sierra).
http://dx.doi.org/10.1016/j.ijhydene.2014.04.078

operating temperature and the electrolyte. However, the proton exchange membrane (PEM) fuel cell has gained more attention by their low operating temperature and high efficiency. The operation of a fuel cell is simple, hydrogen and oxygen are supplied separately to the cell and they react electrochemically to generate electricity, the only products obtained are water and heat. The reactions that take place at the anode and the cathode of the fuel cell are described below:

$$2H_2 \rightarrow 4H^+ + 4e^- \quad (1)$$

$$O_2 + 4H^+ + 4e^- \rightarrow 2H_2O \quad (2)$$

A fuel cell is composed of a membrane, catalyst layers, gas diffusion layers and bipolar plates. The membrane (electrolyte) is a perfluorosulfonic acid commonly called Nafion, which allows the transport of $H^+$ ions from the anode to the cathode, next there are the catalyst layers or electrodes (anode and cathode), the zones were oxidation and reduction reactions take place. The catalyst layers are composed essentially of Vulcan carbon and platinum particles. The electrodes and electrolyte together form the membrane-electrode assembly (MEA), the main component of the fuel cell. Next to the catalyst layers are the gas diffusion layers, which are made of carbon paper or carbon cloth, these are porous zones that allow the uniform distribution of reactant gases over the catalyst layers. Finally, there are the bipolar plates, which are made from graphite and give mechanical support and electrical contact to the fuel cell besides containing channels that supply the reactant gases into the electrochemical device.

In spite of the PEM fuel cell operation can be described in a simple form, its performance is considerably affected by the operating conditions of pressure, temperature and gas composition, as well as the material properties that compose it. These factors influence considerably on the cell potential, the magnitude of the activation overpotential, the ohmic resistance and the mass transport losses that characterize the fuel cell [2].

In recent years there have been many efforts to minimize these losses, through the development of new catalytic materials and different types of novel electrolytes [3,4]; however few studies have been reported on the flow field designs and the bipolar plates [5]. It is important to take into account that the performance of a stack depends on the sum of the performance of all its components and this correlation has not been achieved in a practical way so far. One of the main troubles that arise in the stack is the poor distribution of reactant gases into the cell, which is reflected in a non-uniform distribution of current density, dead zones in the membrane, hot spots, degradation of the membrane-electrode assembly and in general a poor performance of the cell [6]. Although this issue has been given enough attention by using numerical simulation and experimental analysis, there are still too many design alternatives to improve the fuel cell performance.

Recent reports about flow field designs indicate that each channel configuration has advantages and disadvantages, which depend on the operating conditions for which they were designed. The most common designs are classified into serpentine, straight channels, interdigitated, columns, mesh, and cascade designs [6,7]. The flow field with the simplest configuration is the straight channel version, this design works efficiently and causes low pressure drops although requires ideal conditions for good performance, for example, when the flows are not supplied with enough pressure a non-uniform distribution of gases on the catalyst layer is developed. Likewise, any water droplet formed in the flow field blocks the channels. Probably, the most common design used in commercial fuel cells is the serpentine flow field, either with single or multiple channels. In this design the gas flows through the channels circulating throughout the active area of the fuel cell. This configuration increases both, the flow speed and the pressure drop; furthermore it improves the water and heat management by transporting liquid and vapor water through the channels [6,7]. The interdigitated flow field was

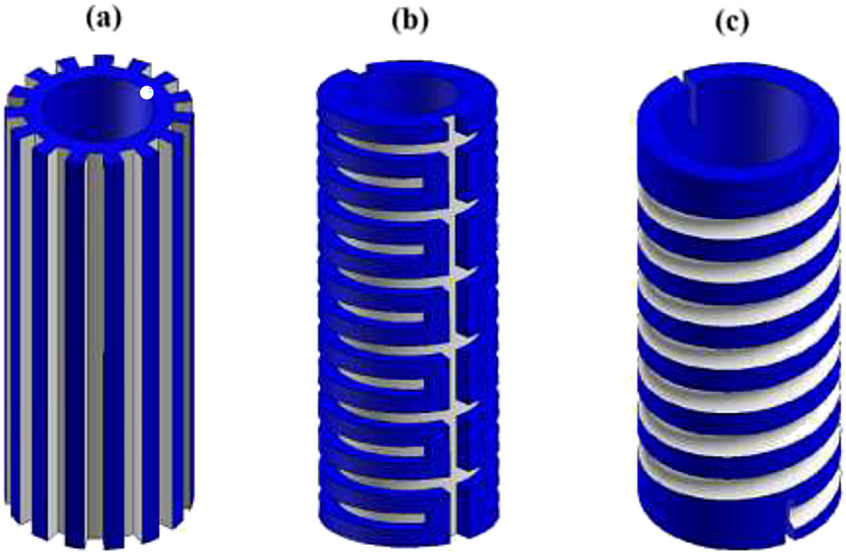


**Fig. 1 – Tubular plates with cylindrical flow fields, a) straight channels, b) interdigitated, c) serpentine.**

designed on a dead-end channel concept, which forces the gases to flow through the gas diffusion layers before they leave the plate. This structure induces forced water removal from the open structure of the gas diffusion layer but it also induces higher pressure drops between the inlet and the outlet than those of the through-flow options [5]. Their advantages and drawbacks were reported in other works [8,9]. The results showed that variants of this design can be applied to enhance its performance.

Besides these channel designs, several variations are being investigated in order to increase the overall efficiency of the fuel cell [6,10]. In this regard, the present work proposes three new versions of conventional flow fields, a) straight channels, b) interdigitated and c) serpentine, which were implemented in a cylindrical geometry and adapted to tubular plates Fig. 1, the goal is to reduce the pressure drops that rectangular flow fields present and homogenize the local species distribution on the catalyst layers of the fuel cell.

## Description of the computational model

The computational model evaluated in this work consists of a cylindrical fuel cell with 5 $cm^2$ active area, including gas diffusion layers (GDL), catalyst layers (CL), membrane (MEM) and monopolar plates (MP). In order to establish the accuracy of the results and to ensure that they were independent of the grid, previous simulations were performed. The reference parameter used to do the analysis was the average current density. The final mesh used in the models had approximately 3.5 million elements. The dimensions of the components, the geometry of the tubular fuel cell and the computational mesh are specified in Table 1 and Fig. 2, respectively.

The assumptions to carry out the numerical simulation of the computational model were the following: (a) stationary and non-isothermal conditions, (b) laminar flow in channels, (c) isotropic porous zones, (d) the electrochemical reactions take place on the catalyst layer surface, (e) transport of species in the gas phase, and (f) the transport of liquid water in the membrane is controlled by diffusion mechanisms and electro-osmotic drag.

### *Mathematical model*

Transport phenomena occurring inside a PEM fuel cell are represented by the governing equations of mass conservation, momentum, energy, species and charge transport. These equations are described below.

**Table 1 – Dimensions of the PEM fuel cell components.**

| Parameter | Unit | Value |
|---|---|---|
| Channel width | mm | 0.8 |
| Channel height | mm | 0.8 |
| Plate thickness | mm | 1.6 |
| Plate height | mm | 20 |
| Average radius | mm | 4.37 |
| Active area | $mm^2$ | 549 |
| GDL thickness | mm | 0.25 |
| CL thickness | mm | 0.02 |
| Membrane thickness | mm | 0.178 |

*Continuity equation*

The continuity equation represents the mass conservation for all transport processes that take place in the fuel cell, such as fluid flow, mass diffusion, phase change and electrochemical reactions. This equation is written in a simplified form (steady state) as:

$$\nabla\cdot(\rho\vec{v}) = S_m \tag{3}$$

where $\rho$ is the fluid density, $\vec{v}$ is the vector velocity and $S_m$ is the source term for the species balance.

*Momentum transport*

The momentum transport equation in a steady state is described by:

$$\nabla\cdot(\rho\vec{v}\vec{v}) = -\nabla p + \nabla\cdot\left(\mu^{\text{eff}}\nabla\vec{v}\right) + S_p \tag{4}$$

where $p$ is the static pressure, $\mu^{\text{eff}}$ is the average viscosity of the mixture and $S_p$ is a source term that contains the physical characteristics of porous media and it is defined as:

$$S_p = -\left(\frac{\mu}{k}\right)\vec{v} \tag{5}$$

where $\mu$ is the gas viscosity (kg/m s), $k$ is the permeability (gas diffusion layers and catalyst layers), and $\vec{v}$ is the superficial vector velocity at the porous media (m/s) [11].

*Species transport*

The species transport equation represents the mass conservation for each individual species of a gas. To determine the local mass fraction of each species $y_i$, the following equation is used:

$$\nabla\cdot(\rho\vec{v}y_i) = -\nabla\cdot\vec{J}_i + S_i \tag{6}$$

where $S_i$ is the source term for each phase, $\vec{J}_i$ is the flux diffusion for the species $i$, which is calculated for a laminar flow as:

$$\vec{J}_i = -\rho D_i\nabla\cdot y_i \tag{7}$$

where $D_i$ is the diffusion coefficient for the species $i$.

*Energy*

The energy equation for steady state is expressed by:

$$\nabla\cdot[\vec{v}(\rho E + p)] = \nabla\cdot\left(k_{\text{eff}}\nabla T - \sum_i h_i\vec{J}_i\right) \tag{8}$$

where $E$ is the total energy, $k_{\text{eff}}$ is the effective conductivity and $\vec{J}_i$ is the flux diffusion for the species $i$.

*Electrochemical model*

The fluid dynamics equations preceding this section were coupled to the electrochemical model using a commercial fuel cell module implemented in Ansys-Fluent®. This set of equations allows to solve the transport phenomena and electrochemical processes occurring in the fuel cell. This model consists of two equations for solving the two potential fields: Equation (9) associated with the transport of electrons

in the catalyst layers, the gas diffusion layers and the plates and, Equation (10) associated to proton transport through the membrane and the catalyst layers.

$$\nabla\cdot(\sigma_{sol}\nabla\varphi_{sol}) + R_{sol} = 0 \tag{9}$$

$$\nabla\cdot(\sigma_{mem}\nabla\varphi_{mem}) + R_{mem} = 0 \tag{10}$$

where $\sigma$ is the electric or ionic conductivity, $\varphi$ is the cell potential and $R$ is the transfer current; the subscripts sol and mem correspond to the solid and the electrolyte phases, respectively.

The transfer current or source terms in Equations (9) and (10) are determined from the general Butler–Volmer formulation, which is used to calculate the local current density on the catalyst layers by the following equations:

$$R_{an} = j_{an}^{ref}\left(\frac{H_2}{H_{2,ref}}\right)^{\gamma_{an}}\left[exp\left(\frac{\alpha_{anF}\eta_{an}}{RT}\right) - exp\left(\frac{\alpha_{caF}\eta_{an}}{RT}\right)\right] \tag{11}$$

$$R_{ca} = j_{ca}^{ref}\left(\frac{O_2}{O_{2,ref}}\right)^{\gamma_{ca}}\left[-exp\left(\frac{\alpha_{an}F\eta_{ca}}{RT}\right) + exp\left(\frac{-\alpha_{ca}F\eta_{ca}}{RT}\right)\right] \tag{12}$$

where $j^{ref}$ is the exchange current density, $H_2/H_{2,ref}$, are the local and reference species concentrations, $\gamma$ is the concentration coefficient, $\alpha$ is the transfer coefficient, $\eta$ is the activation losses defined in Equations (13) and (14), and $F$ is the Faraday constant ($9.65 \times 10^7$ C kg$^{-1}$ mol$^{-1}$).

The reaction kinetics is controlled by the local surface overpotential, $\eta$, known as activation losses, which is associated with the difference of surface potentials between the electrode and the electrolyte $\varphi_{sol}$ and $\varphi_{mem}$. This overpotential is calculated for both the anode and the cathode, including as last term the open circuit voltage ($V_{OC}$) and thus establishing the potential difference between both electrodes.

$$\eta_{an} = \varphi_{sol} - \varphi_{mem} \tag{13}$$

$$\eta_{ca} = \varphi_{sol} - \varphi_{mem} - V_{oc} \tag{14}$$

The membrane is modeled as a porous zone and its properties such as ionic conductivity $\sigma_{mem}$ and the electro-osmotic drag coefficient are evaluated as a function of the water content $\lambda$. These properties are represented by the correlations reported by T. E. Springer et al. [12] (Equations (15)–(17)):

**Table 2 – Operating conditions and electrochemical parameters.**

| Parameter | Symbol | Unit | Value |
|---|---|---|---|
| Pressure | $P$ | atm | 2 |
| Cell temperature | $Tc$ | K | 343 |
| Flow temperature | $Tf$ | K | 343 |
| Relative humidity ($H_2$) | $HR_a$ | % | 50 |
| Relative humidity ($O_2$) | $HR_c$ | % | 100 |
| Ref. exchange current density (anode) | $j_{ref,an}$ | A cm$^{-2}$ | 0.2 |
| Ref. exchange current density (cathode) | $j_{ref,ca}$ | A cm$^{-2}$ | $1 \times 10^{-4}$ |
| Charge transfer coefficient (anode) | $\alpha_{,an}$ | – | 2 |
| Charge transfer coefficient (cathode) | $\alpha_{,ca}$ | – | 2 |
| Concentration exponent (anode) | $\gamma_{,an}$ | – | 0.5 |
| Concentration exponent (cathode) | $\gamma_{,ca}$ | – | 1 |
| GDL porosity | $\varepsilon_{GDL}$ | – | 0.4 |
| GDL viscous resistance | $\upsilon_{R,GDL}$ | 1/m$^2$ | $1 \times 10^{12}$ |
| CL porosity | $\varepsilon_{CL}$ | – | 0.2 |
| CL viscous resistance | $\upsilon_{R,CL}$ | 1/m$^2$ | $4 \times 10^{12}$ |

$$\sigma_{mem} = (0.00514\lambda - 0.00326)e^{1268\left(\frac{1}{303}-\frac{1}{T}\right)} \tag{15}$$

$$\lambda = 0.043 + 17.81a - 39.84a^2 + 36a^3 (a < 1) \tag{16}$$

$$\lambda = 14 + 1.4(a-1)(a > 1) \tag{17}$$

where $a$ is the water activity. The saturation model reported by T. Nguyen [13] and J. H. Nam et al. [14]. is used to model the formation and transport of liquid water in the membrane-electrode assembly.

From these Equations (9)–(16) both potential fields are solved, also the electrochemical process that causes the three potential losses in a fuel cell are included, which are known as: activation overpotential, ohmic overpotential and concentration overpotential.

The operating conditions and the electrochemical parameters used in the simulation were taken from experimental data and literature data [15–18]. These values are shown in Table 2.

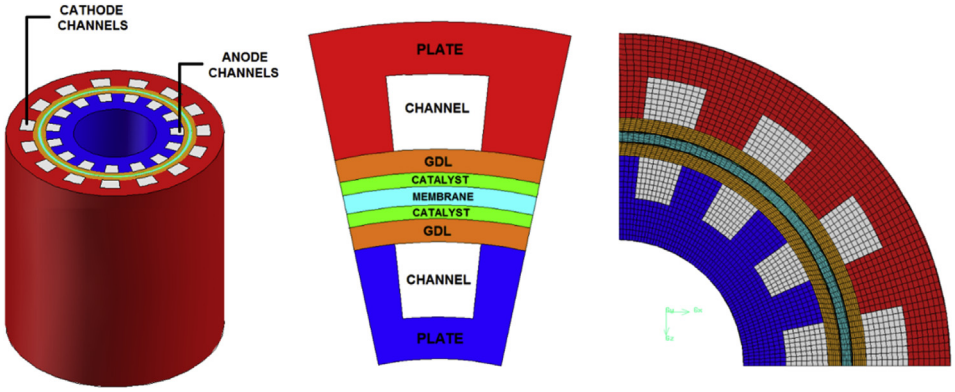


**Fig. 2 – Design of a tubular PEM fuel cell (left), components (center) and computational grid (right).**

*Boundary conditions*

The boundary conditions applied to the computational domain were (1) mass flow inlet, (2) pressure outlet, (3) constant potential at anode and, (4) variable potential at cathode, which were set to calculate the current density in the cell. The flows of hydrogen and oxygen were fed in the same direction in order to obtain uniform current density distributions as well as reported by J. M. Sierra et al. [19]. The mass flow rates were calculated for an active area of 5 $cm^2$ with a stoichiometry of 1.25 and 2 for the anode and the cathode, respectively. Likewise, the concentrations of hydrogen and oxygen flows were determined, they were supplied at 2 atm of pressure and 343 K of temperature, with 50% and 100% of relative humidity for the anode and the cathode, respectively. From these boundary conditions, the fluid dynamics equations and the electrochemical model of Ansys-Fluent®, the computational model of PEM fuel cell was solved. A segregated method, the first order scheme and SIMPLE algorithm were used to solve the equations [11]. The model was evaluated in different operating potentials and thereby the current density was calculated. Using these data, polarization curves were generated to evaluate the performance of each flow field.

## Results and discussion

In this section the numerical results for different models of PEM fuel cell are presented. Likewise, a comparison between tubular and conventional flow-fields with the same active area of 5 $cm^2$ is realized. The results are presented by distribution contours of pressure, species concentration, proton conductivity, temperature and current density, which provide relevant information about the processes that take place inside the fuel cell. The contours were obtained at 0.6 V and they are displayed in the following interfaces: gas diffusion layer - catalyst layer (GDL/CL), catalyst layer – membrane (CL/MEM) and bipolar plates (PB) for terminals, anode and cathode.

### *Pressure*

The results of pressure drops (Pa) for cylindrical and conventional flow fields are illustrated in Fig. 3. Pressure distributions are presented at the cathode interface (GDL/CL) for three designs: straight channels, interdigitated and, serpentine. The straight channels design, see Fig. 3a, showed the smallest pressure drops with values up to 0.27 Pa, followed by the interdigitated design, see Fig. 3b, with 5.14 Pa and finally the serpentine, see Fig. 3c, with 28.3 Pa. Although the interdigitated design has a discontinuity in the channels and increases the pressure drops, the predominant factor was the channel length, as it is observed in the serpentine design values. Moreover, a comparison between the anode and the cathode for each design revealed that the pressure at the anode decreases as the voltage decreases because the hydrogen must satisfy the current demanded by the cell. On the contrary, the gas pressure at the cathode increases as the voltage decreases

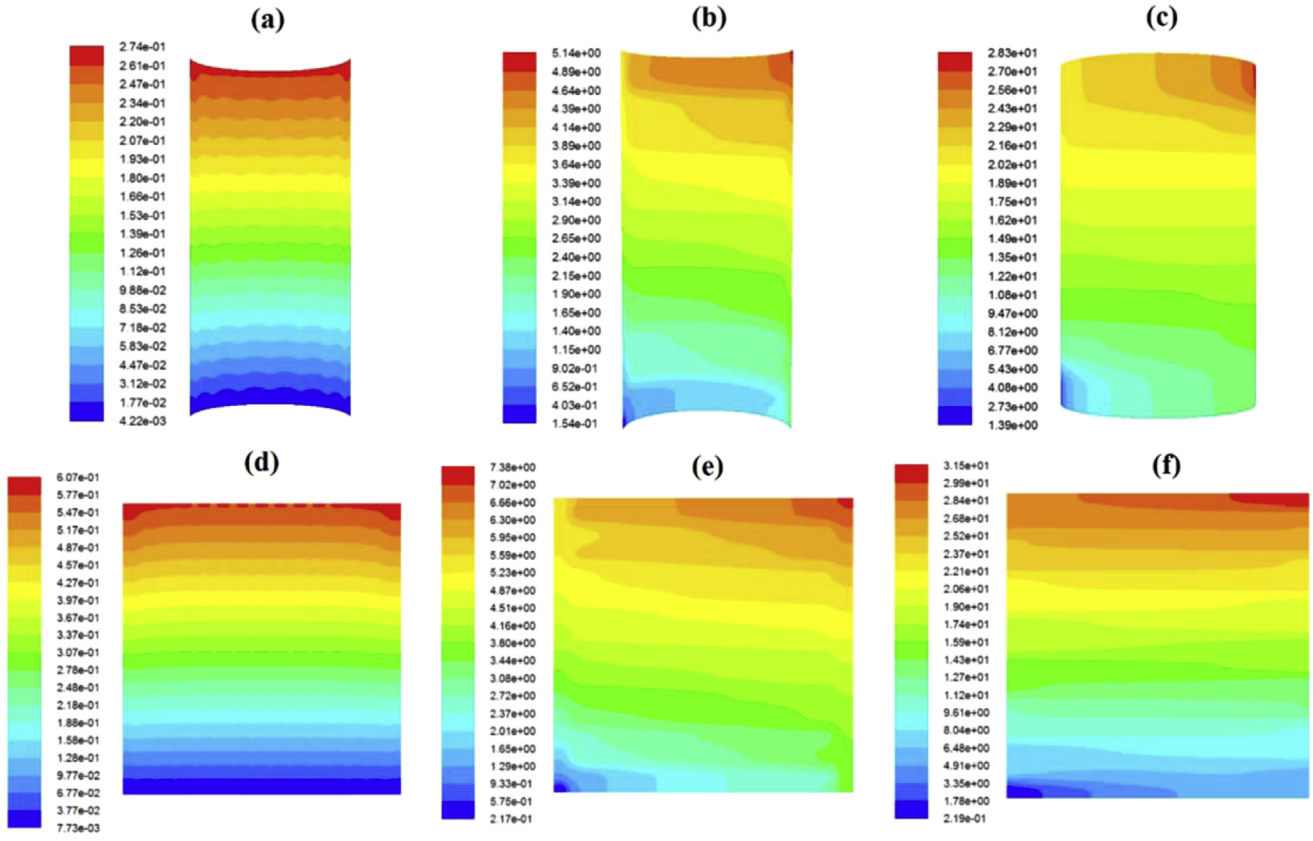


**Fig. 3 – Pressure distributions (Pa) at the cathode interface GDL/CL for tubular designs: a) straight channels, b) interdigitated, c) serpentine, and conventional designs: d) straight channels, e) interdigitated and f) serpentine.**

due to the water generation in the electrode that causes a pressure rising in the flow channels. A comparison with conventional designs (Fig. 3d, e, f) was also performed and the same distribution pattern was observed, however the pressure drops were higher than those of the tubular designs, showing values up to 0.6, 7.38 and 31.5 Pa for straight channels, interdigitated and serpentine designs, respectively.

If a single comparison of each tubular design with the equivalent conventional design is performed, the pressure differences are attributed to the shape of the channels; for conventional designs the channel profile is completely rectangular and flow channels are shifted on a one-dimensional trajectory; however, for the tubular designs (Fig. 3a, b, c) channel profile and trajectory vary for each one. For the straight channels flow-field, the channel profile is slightly trapezoidal, having a channel width of 1.15 mm for the first base and 0.98 mm for second base. This is the cause of pressure variations between conventional design and tubular design. For the interdigitated flow field Fig. 3b, flow goes through a circular path, being the predominant factor. In the case of the tubular serpentine Fig. 3c, both features are critical, hemispherical profile of the channel and the spiral flow path, reducing of this way the pressure drop by 10%. Hence the cylindrical flow fields reduce the pressure drops more efficiently compared to the conventional designs.

### *Hydrogen concentration*

The distribution of gases through the catalyst layers is a factor used to examine the performance because it affects the current density produced. A uniform gas distribution will extend the lifetime of the MEA and will enhance the performance of the cell. Fig. 4 shows the distribution contours of the hydrogen concentration for different flow fields. The results are presented at the anode interface (GDL/CL) for an operating voltage of 0.6 V. The distribution contours show that the hydrogen concentration is higher at the inlet and decreases as it moves into the channel due to the fuel consumption in the cell. Furthermore, it may also be observed that tubular designs with straight channels and serpentine (Fig. 4a and c) have a more uniform concentration of hydrogen in the active area of the cell. This is due to the characteristics of the flow channels; the designs with straight channels are favored by the multichannel supply, allowing a uniform gas distribution in each zone of the cell. This concept is used in the flow field of stacks. Moreover, the tubular serpentine design presented homogeneous distributions of hydrogen in the active area due to hemispherical channel profile and the helicoidal flow path. In the case of the interdigitated flow fields, these did not favor the distribution of hydrogen within the fuel cell, the forced convection causes the reactant gas reacts only in the region near the feeding zone.

### *Oxygen concentration*

The oxygen concentration distributions for the different fuel cell designs are shown in Fig. 5. The results are presented at the (GDL/CL) cathode interface for an operating voltage of 0.6 V. As it is seen, the oxygen concentration is high at the inlet channels and gradually decreases as it moves through the channels until reaching the outlet. However, interdigital designs show a different distribution, the lower oxygen concentration is in the central part where the outlet channels are located. This variation is due to the increased concentration of

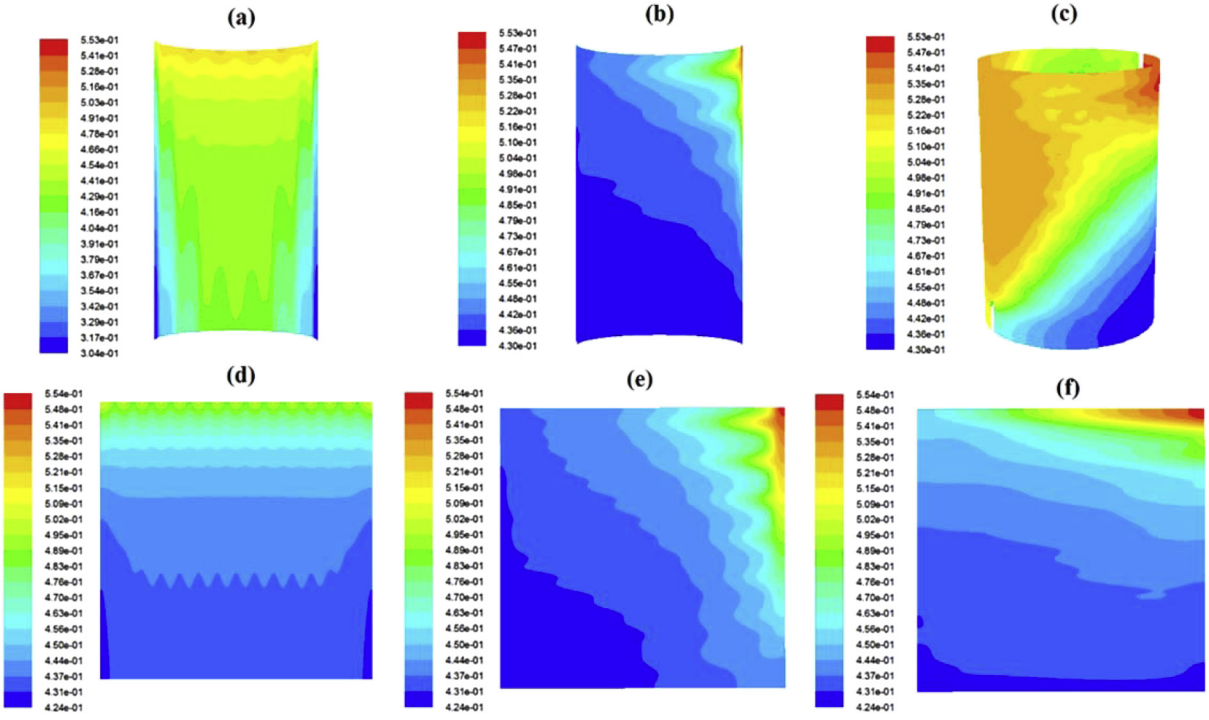


**Fig. 4 – Contours of the mass fraction of hydrogen at the anode interface (GDL/CL) for tubular designs: a) straight channels, b) interdigitated, c) serpentine, and conventional designs: d) straight channels, e) interdigitated and f) serpentine.**

water in the cell by the cathode reaction, which reduces the oxygen concentration in this area. The distribution patterns for both tubular and conventional designs are similar in both cases.

### *Water concentration*

The water concentration distributions for different flow fields are presented in Fig. 6. Once again, the results are shown at the (GDL/CL) interface of the cathode. As it is seen in the distribution contours, the concentration of water is opposite to the oxygen concentration, the lower water concentration occurs at the entrance of the channels and the largest water concentration at the outlet. The interdigitated design is characterized by its efficiency to expel water using forced convection and its effects can be clearly seen in Fig. 6b and e. Likewise, it should be noted that a water concentration analysis was performed at different cell potentials and showed that the concentration of water increases as the current density increases. The interdigital designs have the highest concentrations of water, followed by the parallel channel designs and then the serpentines.

### *Proton conductivity*

The ionic conductivity of the membrane is strongly linked to its structure and its water content. If the membrane is not sufficiently hydrated there will not be an effective ion transport from anode to cathode of the cell, which would affect its performance. But if the membrane is too hydrated this could flood the catalyst layers, which would affect the transport of gases and the reactions at the triple-phase of the electrodes. The water content of the membrane must be maintained in certain ranges ($\lambda = 14$). Fig. 7 shows the proton conductivity contours at the cathode interface (CL/MEM) for the flow fields. These results were normalized to the same scale for comparison between the different designs. As shown in the figures, the ionic conductivity of the membrane is low in the zones close to the inlet and high in zones near the outlet, this is due to that ionic conductivity is closely related with the water generation in the fuel cell [20]. And as well as interdigital designs had the highest water concentration values, also presented the highest values of ionic conductivity, improving of this way the hydration of the membrane.

### *Temperature*

Temperature plays a key role in the performance of the fuel cell as it affects all transport processes that take place at the MEA. The main parameters affected by temperature are: the gas composition, the exchange current density, the conductivity of the membrane and the gas diffusivity. The temperature contours for the different flow field designs are shown in Fig. 8. These results are presented at the anode interface (GDL/CL) for an operating voltage of 0.6 V. In the figure it is observed that the higher values of temperature are presented in the ribs and the lower values in the channels. These temperature variations are mainly attributed to the exothermic reactions taking place in the catalyst layers and the ohmic heating in the plates. Because the flows and the external temperature of the

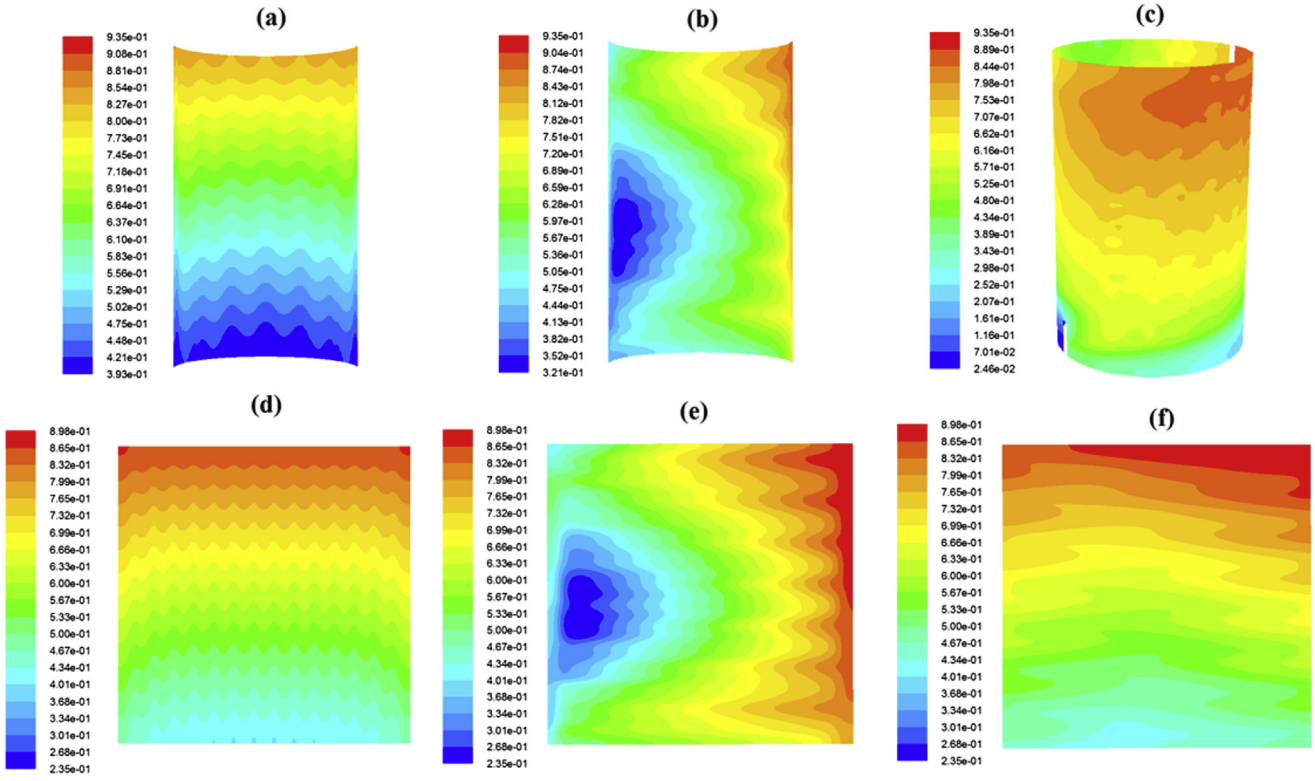


**Fig. 5 – Contours of the mass fraction of oxygen at the cathode interface (GDL/CL) for tubular designs: a) straight channels, b) interdigitated, c) serpentine, and conventional designs: d) straight channels, e) interdigitated and f) serpentine.**

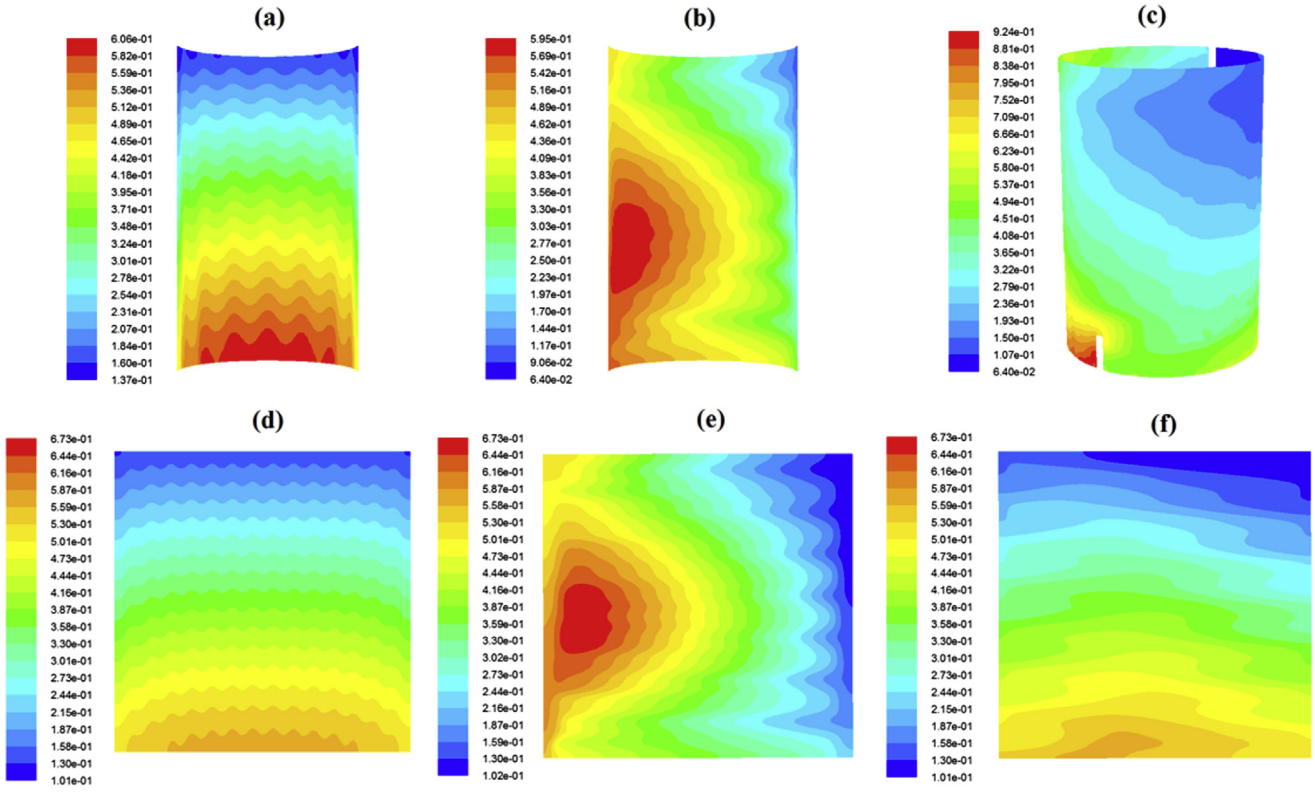


**Fig. 6 – Contours of the mass fraction of water at the cathode interface (GDL/CL) for tubular designs: a) straight channels, b) interdigitated, c) serpentine, and conventional designs: d) straight channels, e) interdigitated and f) serpentine.**

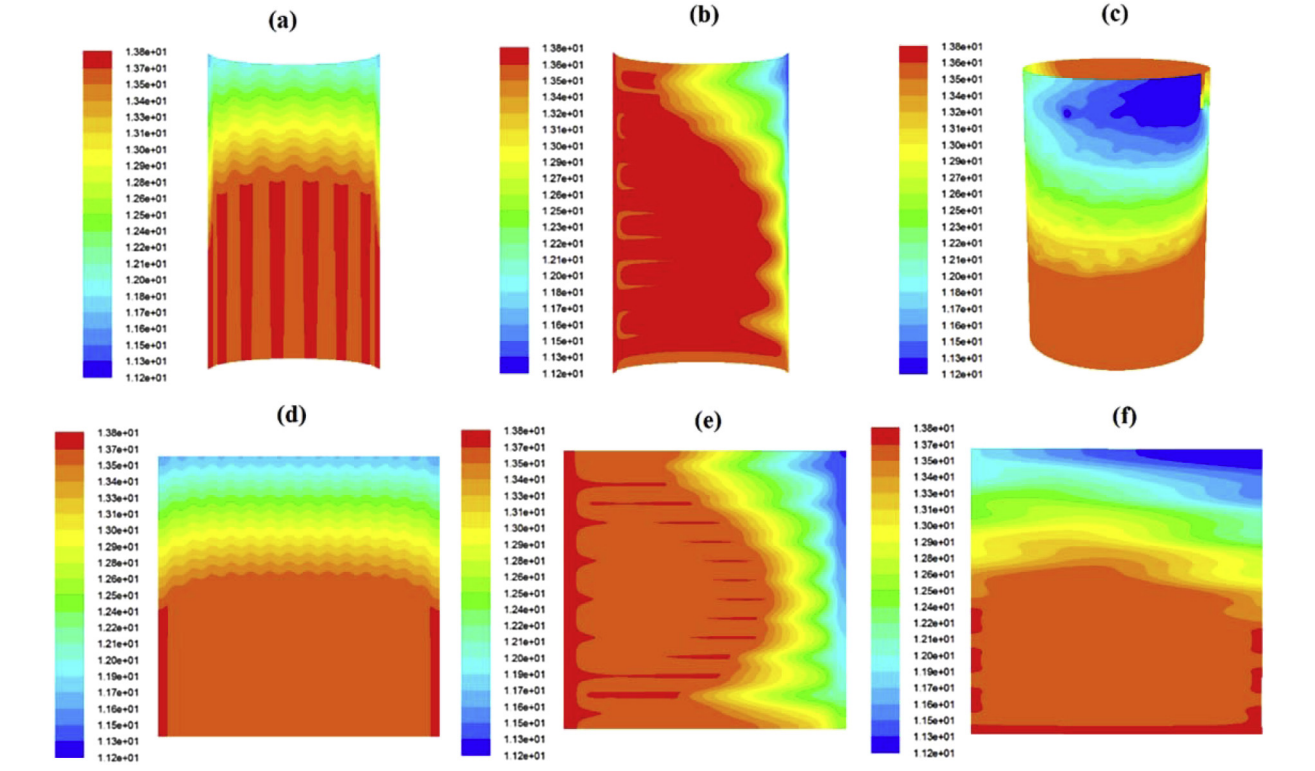


**Fig. 7 – Proton conductivity distributions (ohm$^{-1}$ m$^{-1}$) at the cathode interface CL/MEM for tubular designs: a) straight channels, b) interdigitated, c) serpentine, and conventional designs: d) straight channels, e) interdigitated and f) serpentine.**

plates were kept at 343 K, the temperature variations inside the cell was less than 2 K. The design exhibiting the largest temperature variation was the conventional serpentine design, $\Delta T = 1.7$ K, and design that had the lowest temperature variation was the tubular serpentine, $\Delta T = 0.5$ K.

### *Current density*

The current density distributions of different flow fields at 0.6 V of operating voltage are shown in Fig. 9. The results were normalized at the same scale of current density to carry out a comparative analysis. These results indicate that the current density adopts the same distribution pattern of channel configurations, however the highest current density was observed in the ribs of the plate and the lowest in the channels. Furthermore, the serpentine design Fig. 9c displayed the most uniform current density distributions. Subsequently a comparison between conventional and tubular designs was performed, similar current density distributions were also observed. However, the tubular serpentine design showed the most homogeneous values of current density on the entire active area of the fuel cell. This is due to the gradual reduction of the angle in the flow path and the three-dimensional twist of the channel that improved the mass transport processes and in turn were reflected in the reduction of pressure drops along the channel, the uniform distribution of reactant gases on the catalyst layers as well as the enhancement of water removal from porous media and the flow channels.

Fig. 10 illustrates the polarization curves obtained for all the flow field designs. It is seen that the performance of the three designs was similar under a normal operating range. At high operating potentials the activation losses were followed by ohmic losses with a linear behavior; when the potential was below 0.6 V the mass transport losses were present. Under these operating conditions, 2 atm, 343 K and, 50 and 100% of relative humidity in the flows, the parallel channel design performed slightly better than the other designs. This result was obtained because the gas supply was done individually for each channel, which favored the magnitude of the current density. If the reactant gases are fed only by a single channel their performance is affected considerably [21]. However, the serpentine tubular design showed the most uniform current density distributions, so it could be considered for studying the degradation of the membrane-electrode assembly as well as being subjected to continuous cycles of loading and unloading.

Fig. 11 shows a comparison between the polarization curves of the tubular designs and the conventional designs, and referencing the polarization curve for the serpentine flow field, which was obtained by numerical simulation in this work and was validated with data reported in literature [7,22]; it is seen that the polarization results had a comparable behavior in both cases with the difference that the conventional flow fields showed the highest values of current density almost over the entire operating range. The differences are attributed to the mass transport processes, which occur more homogeneously in the tubular flow fields than in the

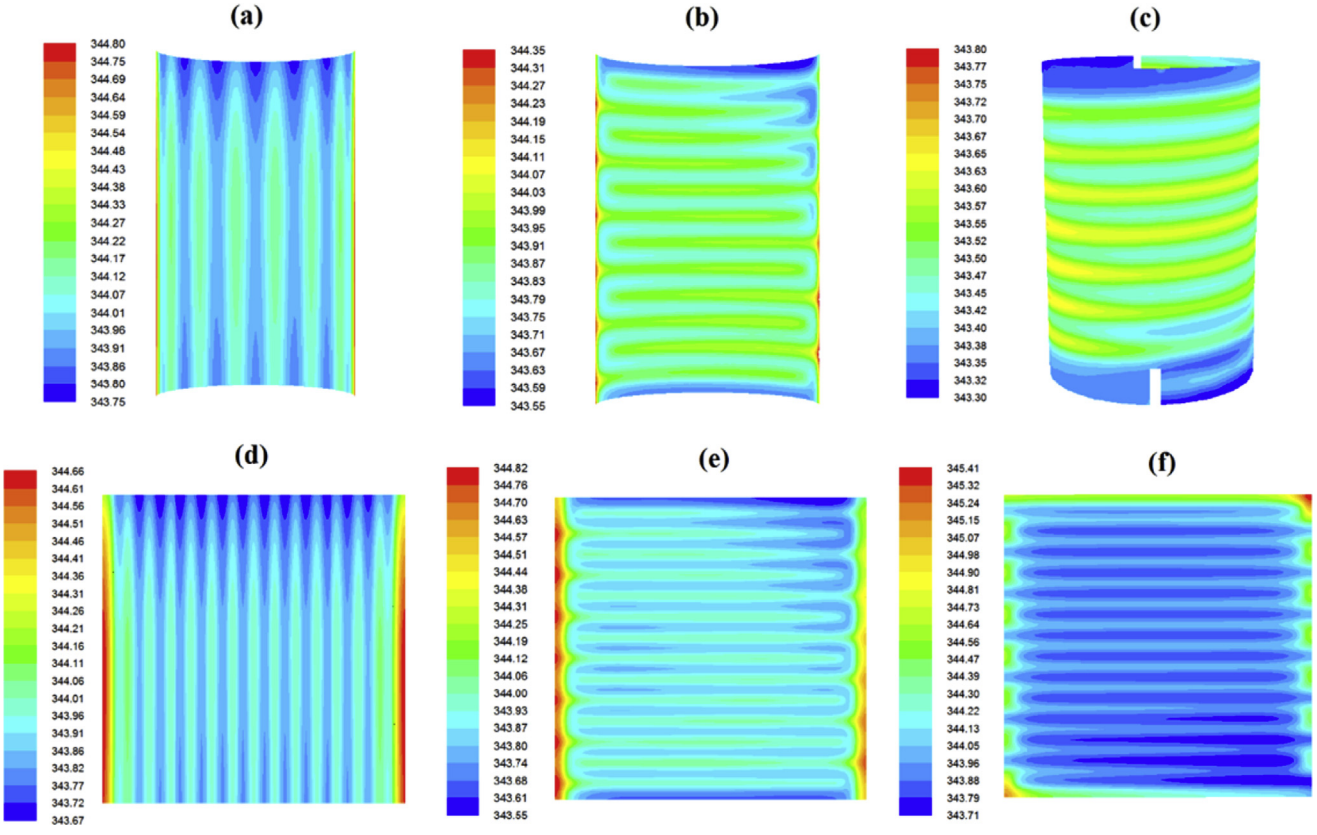


**Fig. 8 – Temperature distributions at the anode interface (GDL/CL) for tubular designs: a) straight channels, b) interdigitated, c) serpentine, and conventional designs: d) straight channels, e) interdigitated and f) serpentine.**

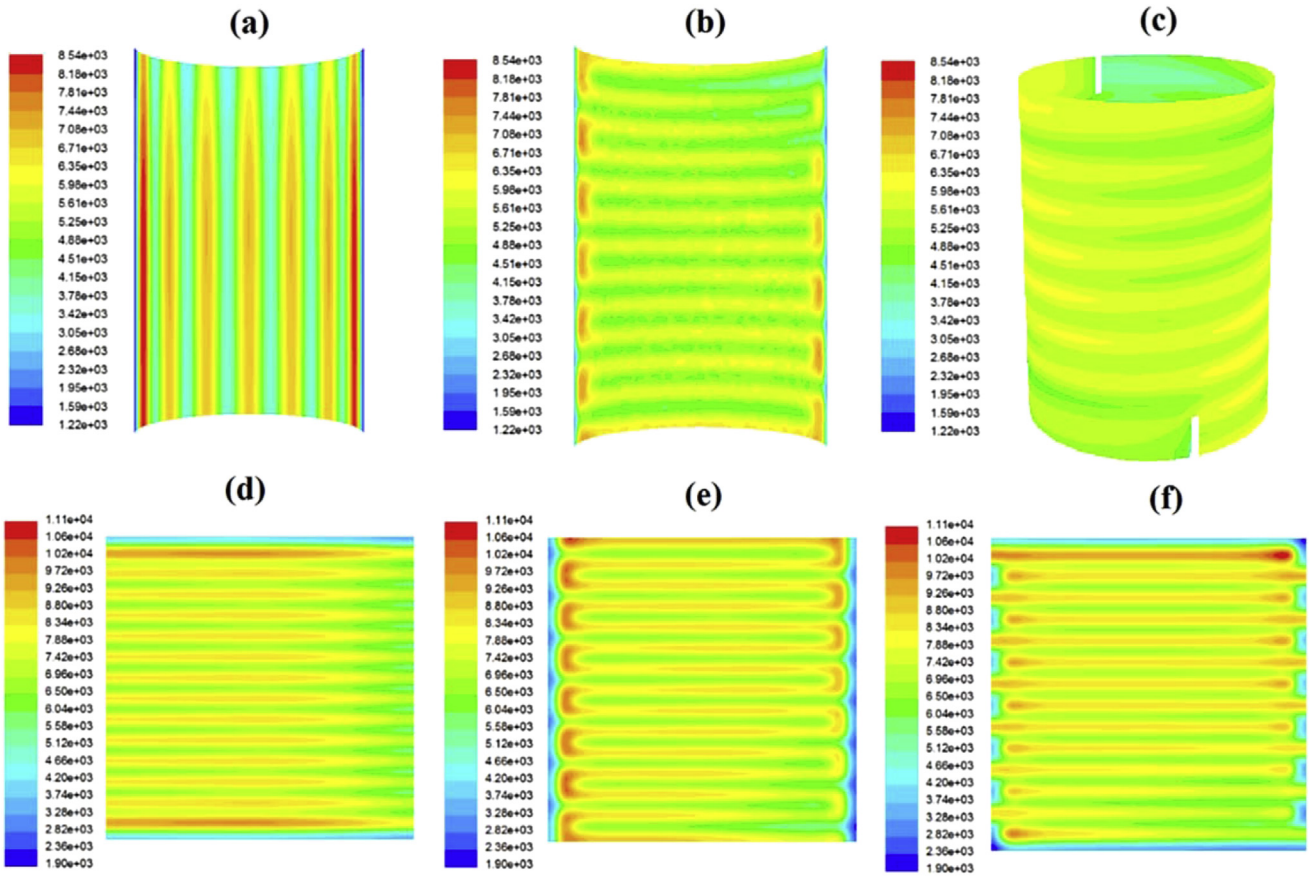


**Fig. 9 – Current density distributions (A/m$^2$) at the cathode plate for tubular designs: a) straight channels, b) interdigitated, c) serpentine, and conventional designs: d) straight channels, e) interdigitated and f) serpentine.**

conventional flow fields in accordance with the species concentration in the catalyst layers, the pressure drops in the channels and the local distributions of current density shown in Figs. 3–11. If uniform (homogenous) mass transport processes at the anode and the cathode are pursued, they will be reflected mainly in lower current density values. Hence the tubular designs could perform in a better way this function. In contrast, if higher current density values want to be obtained, it would be appropriate to rely on the conventional designs although this would involve high pressure drops in the channels and non uniform local species distributions that would considerably affect the overall performance of the MEA.

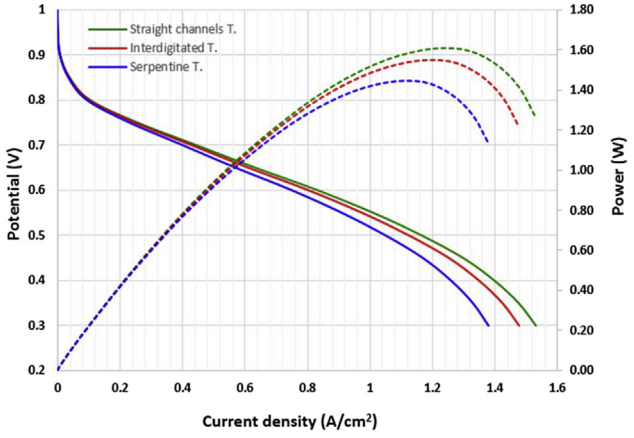


**Fig. 10 – Comparison of the polarization curves (solid lines) and the power plots (dashed lines) of different flow fields.**

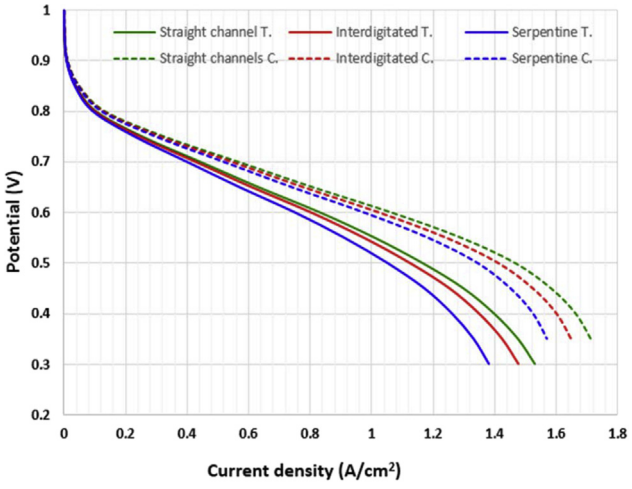


**Fig. 11 – Polarization curves for the tubular (solid lines) and the conventional (dashed lines) designs.**

## Conclusions

A computational fluid dynamics study on a PEM fuel cell was carried out in order to evaluate the performance of three conventional flow fields adapted to tubular plates. From the solution of the fluid dynamics equations and the electrochemical model of the commercial CFD code, distribution contours of different variables and polarization curves were obtained. The distribution contours allowed a local analysis of transport phenomena, which showed that the tubular designs exhibit more uniform distributions of pressure, hydrogen and oxygen concentration and current density, than the conventional flow fields, highlighting the advantages and disadvantages of each design. It is worth noting that the tubular design with the straight channels presented the lowest pressure drop in the flow channels, which was also reflected in a higher water accumulation at the cathode, an increase in the ionic conductivity of the membrane and therefore a rise in the current density in comparison with the other designs; the interdigitated tubular design had the highest water generation at the cathode, which also caused an increase in the ionic conductivity of the membrane and the current density in the cell; however, the serpentine design presented the most uniform distributions of hydrogen concentration, temperature and current density on the active area of the cell.

The global performance of the flow fields observed in the polarization curves indicates that despite exhibiting non uniform distributions of species and current, the conventional designs present higher values of current density when are compared to the tubular designs. In this regard, the serpentine tubular design displayed the most uniform distributions of current density over the entire active area of the cell which make it promising for being built and tested experimentally, thus increasing the lifetime of the membrane-electrode assembly and preventing its degradation. Hence, the tubular designs may be considered as potential alternatives for the current designs of the fuel cell, especially for portable applications.

## Acknowledgments

The author gratefully acknowledges to Renewable Energy Institute – UNAM for the granted support to perform the numerical simulations in their computing equipment and the use of Ansys-Fluent® software license.

## Nomenclature

| | |
|---|---|
| $a$ | water activity |
| $D$ | diffusion coefficient, $m^2\ s^{-1}$ |
| $F$ | Faraday constant, 96,487 C $mol^{-1}$ |
| $h$ | enthalpy, J |
| $j$ | exchange current density, A $m^{-2}$ |
| $J$ | flux diffusion, kg $m^{-2}\ s^{-1}$ |
| $k$ | permeability, $m^{-2}$ |
| k | effective conductivity, $Wm^{-1}\ K^{-1}$ |
| $p$ | pressure, Pa |
| $R$ | transfer current, A $m^{-3}$ |
| R | universal gas constant, 8.314 J $K^{-1}\ mol^{-1}$ |
| $T$ | temperature, K |
| $v$ | velocity m $s^{-1}$ |
| y | mass fraction species |

*Greek symbols*

| | |
|---|---|
| $\alpha$ | transfer coefficient |
| $\varepsilon$ | porosity |
| $\rho$ | density, kg $m^{-3}$ |
| $\gamma$ | concentration coefficient |
| $\eta$ | over-potential, V |
| $\mu$ | dynamic viscosity, kg $m^{-1}\ s^{-1}$ |
| $\sigma$ | electric or ionic conductivity, $ohm^{-1}\ m^{-1}$ |
| $\varphi$ | cell potential, V |

*Subscripts/superscripts*

| | |
|---|---|
| an | anode |
| ca | cathode |
| mem | membrane |
| sol | solid |
| ref | reference |
| eff | effective |
| m | mass |
| p | porous |
| $i$ | reference to individual species. |

## REFERENCES

[1] Rifkin Jeremy. The hydrogen economy. New York: Penguin Putman Inc.; 2000.
[2] Larminie J, Dicks A. Fuel cells systems explained. 2nd ed. Wiley; 2003.
[3] Santiago AA, Vargas J, Cruz-Gómez J, Tlenkopatchev MA, Gaviño R, López-González M, et al. Synthesis and ionic transport of sulfonated ring-opened polynorbornene based copolymers. Polymer 2011;52:4208–20.
[4] Santiago AA, Vargas J, Tlenkopatchev MA, López-González M, Riande E. Electrochemical performance of membranes based on hydrogenated polynorbornenes functionalized with imide side groups containing sulfonated fluorinated moieties. J Membr Sci 2012;403–404:121–8.
[5] Hoogers G. Fuel cell technology handbook. New York: CRC Press; 2002.
[6] Manso AP, Marzo FF, Barranco J, Garikano X, Garmendia Mujika M. Influence of geometric parameters of the flow fields on the performance of a PEM fuel cell. A review. Int J Hydrogen Energy 2012;37:15256–87.
[7] Barbir F. PEM fuel cells – theory and practice. Academic Press, Elsevier; 2005.
[8] Nam Jin Hyun, Lee Kyu-Jin, Sohn Sangho, Kim Charn-Jung. Multi-pass serpentine flow-fields to enhance under-rib convection in polymer electrolyte membrane fuel cells: design and geometrical characterization. J Power Sources 2009;188:14–23.
[9] Li Xianguo, Sabir Imran. Review of bipolar plates in PEM fuel cells: flow-field designs. Int J Hydrogen Energy 2005;30:359–71.
[10] Ramos-Alvarado Bladimir, Hernandez-Guerrero Abel, Juarez-Robles Daniel, Li Peiwen. Numerical investigation of the performance of symmetric flow distributors as flow channels for PEM fuel cells. Int J Hydrogen Energy 2012;37:436–48.
[11] Fluent 6.3 – fuel cells module manual; 2007.

[12] Springer TE, Zawodzinski TA, Gottesfeld S. Polymer electrolyte fuel cell model. J Electrochem Soc 1991;138:2334–42.
[13] Seok Yi Jung, Van Nguyen Trung. Multicomponent transport in porous electrodes of proton exchange membrane fuel cells using the interdigitated gas distributors. J Electrochem Soc 1999;146:38–45.
[14] Nam JH, Kaviany M. Effective diffusivity and water-saturation distribution in single- and two-layer PEMFC diffusion medium. Int J Heat Mass Transf 2003;46:4595–611.
[15] Shimpalee S, Greenway S, Van Zee JW. The impact of channel path length on PEMFC flow-field design. J Power Sources 2006;160:398–406.
[16] Djilali N, Nguyen PT, Berning T. Computational model of a PEM fuel cell with serpentine gas flow channels. J Power Sources 2004;130:149–57.
[17] Berning T, Djilali N. Three-dimensional computational analysis of transport phenomena in a PEM fuel cell, a parametric study. J Power Sources 2003;124:440–52.
[18] Um S, Wang CY. Three-dimensional analysis of transport and electrochemical reactions in polymer electrolyte fuel cells. J Power Sources 2004;125:40–51.
[19] Sierra JM, Moreira J, Sebastian PJ. Numerical analysis of the effect of different gas feeding modes in a proton exchange membrane fuel cell with serpentine flow-field. J Power Sources 2011;196:5070–6.
[20] Sierra JM, Sebastian PJ, Gamboa SA. Study of activation losses and ohmic resistance in a PEM fuel cell using computational fluid dynamics. ECS Trans 2009;20(1):395–405.
[21] Weng Fang-Bor, Su Ay, Jung Guo-Bin, Chiu Yen-Chiao, Chan Shih-Hung. Numerical prediction of concentration and current distributions in PEMFC. J Power Sources 2005;145:546–54.
[22] Juarez-Robles Daniel, Hernandez-Guerrero Abel, Ramos-Alvarado Bladimir, Elizalde-Blancas Francisco, Damian-Ascencio Cesar E. Multiple concentric spirals for the flow field of a proton exchange membrane fuel cell. J Power Sources 2011;196:8019–30.